How to cite: *Angew. Chem. Int. Ed.* **2025**, e25258
doi.org/10.1002/anie.202525258

Chemical Reaction Network

Comprehensive Mapping of Compositional Dynamics in the Formose Reaction Network

*Hiroaki Nishijima, Hiro Tabata, Yoko Hase, Rika Miyake, and Shuji Nakanishi**

Abstract: A chemical reaction network (CRN) can generate complex molecules from simple starting materials through multiple interconnected reactions. The formose reaction, which produces monosaccharides from formaldehyde (HCHO), is a prototypical non-enzymatic CRN. Although more than half of the feedstock in this reaction is converted into non-target products (products other than the target monosaccharides), traditionally referred to as "tar," the compositional evolution of these products has remained unexplored. In this study, we visualized the formose reaction's compositional landscape (target and non-target products) by applying van Krevelen (VK) diagrams and Kendrick mass defect (KMD) plots using data from high-resolution mass spectrometry, enabling comprehensive visualization of the products' composition without structural identification of individual compounds. Under NaOH catalysis, various side reactions proceeded with low selectivity, leading to a wide variety of non-target products, whereas under $Ca(OH)_2$ catalysis, dehydration-type side reactions became predominant in the later stages. These findings reveal that the product distribution in the formose reaction is highly catalyst- and stage-dependent. The developed visualization framework provides a powerful tool for understanding complex CRNs and suggests rational strategies for reaction control, such as suppressing dehydration to improve the yield of target products in the presence of $Ca(OH)_2$ catalyst.

Chemical reaction networks (CRNs), which generate complex molecules from simple starting materials through multiple interconnected reactions, have attracted growing interest in recent years.[1–7] The formose reaction, which produces monosaccharides from formaldehyde (HCHO) (Figure 1a),[8] is a prototypical example of a non-enzymatic CRN and has contributed significantly to the advancement of related research.[9–11] In this reaction system, various reactions—including aldol and retro-aldol reactions, isomerization, and disproportionation—proceed in parallel under basic conditions starting from HCHO. Notably, even in the absence of enzymes, monosaccharides are formed autocatalytically. Several reaction pathways have been proposed, including the Breslow autocatalytic reaction cycle, which involves the regeneration of glycolaldehyde.[12–16] Because of this non-enzymatic formation of monosaccharides, the formose reaction has long been regarded as a plausible prebiotic pathway for sugar production.[17–21] More recently, it has attracted attention as a potential carbon fixation route for converting HCHO (obtained via CO_2 reduction) into sugars.[22–25] Detailed analyses of the monosaccharides produced, including branched-chain monosaccharides, have revealed that the product distribution strongly depends on the catalyst species and reaction conditions.[11]

In the formose reaction, monosaccharides are generally set as the target products; however, they constitute only a subset of the products within the CRN. In fact, the yield of monosaccharides strongly depends on the reaction conditions, and in typical base-catalyzed systems, it can remain below 50%;[26,27] thus, more than half of the feedstock is converted into non-target products. These non-target products are highly diverse, and the separation and identification of their isomers is often infeasible because of the lack of available standards. Consequently, previous studies have collectively referred to these complex mixtures as "tar,"[14,27–29] and their detailed chemical compositions have remained unexplored. However, achieving higher yields of target products generally requires a comprehensive understanding of the overall dynamics of the CRN, including not only the pathways leading to target products but also the formation behavior of

[*] H. Nishijima, Dr. H. Tabata, R. Miyake, Prof. Dr. S. Nakanishi
Research Center for Solar Energy Chemistry, Graduate School of Engineering Science, The University of Osaka, 1–3 Machikaneyama, Toyonaka 560–8531, Japan
E-mail: nakanishi.shuji.es@osaka-u.ac.jp

Dr. H. Tabata
Presidential Endowed Chair for "Platinum Society", The University of Tokyo, 7-3-1 Hongo, Bunkyo-ku, Tokyo 113–8656, Japan

Dr. Y. Hase
Toyota Central R&D Labs. Inc., Yokomichi, Nagakute, Aichi 480–1192, Japan

Prof. Dr. S. Nakanishi
Innovative Catalysis Science Division, Institute for Open and Transdisciplinary Research Initiatives (ICS-OTRI), The University of Osaka, Suita, Osaka 565–0871, Japan

Additional supporting information can be found online in the Supporting Information section

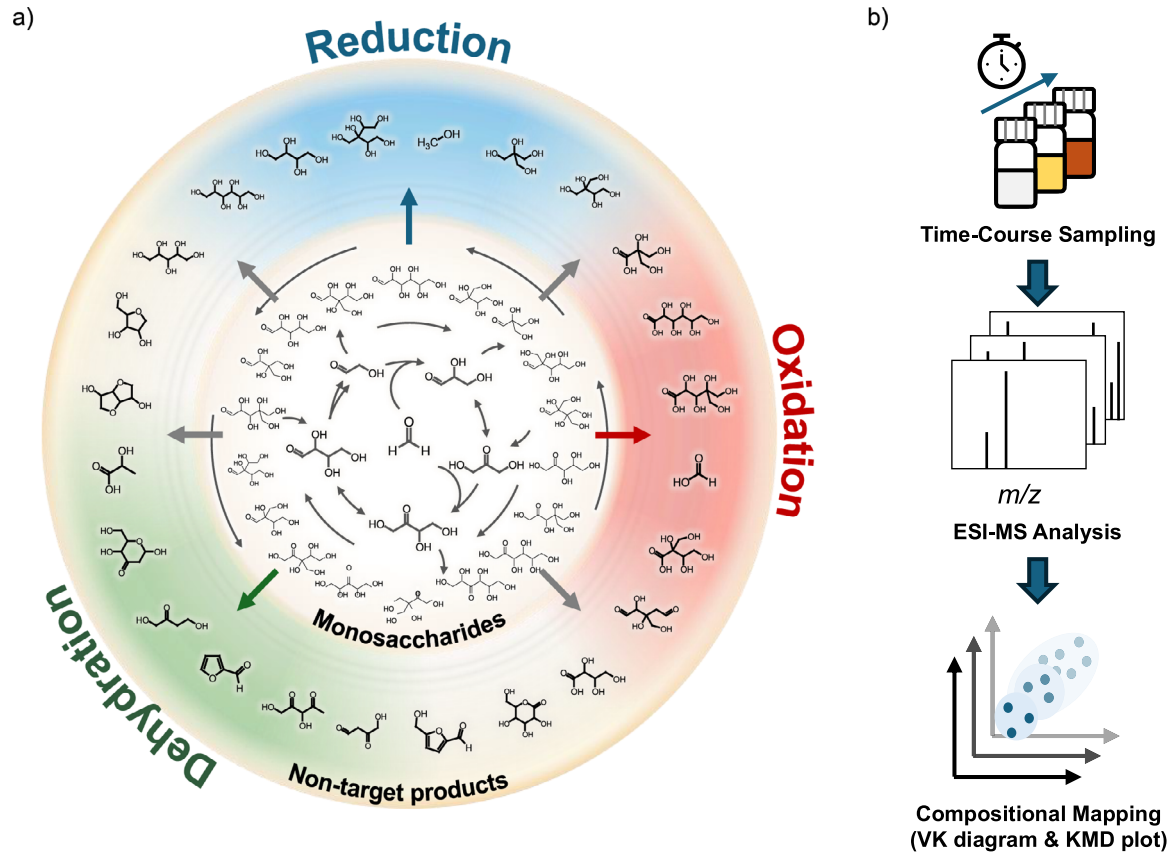

Figure 1. Overview of the formose reaction and analysis workflow. a) The central circle illustrates the formation of target products ($C_nH_{2n}O_n$) via the Breslow cycle. The surrounding ring represents the diverse non-target products, with colored zones highlighting key side-reaction pathways: reduction (blue), dehydration (green), and oxidation (red). Note that the chemical structures shown are illustrative examples of plausible products and have not been individually confirmed. b) Schematic of the experimental and data analysis workflow.

non-target products.[30,31] For example, in oscillatory CRNs, even seemingly irrelevant side reactions can decisively influence the overall system dynamics.[30] In ethylene oxychlorination, analyzing the whole reaction network (including side products) revealed target/byproduct interrelationships, guiding rational catalyst design and process optimization.[31] Thus, to improve the yield of monosaccharides, it is essential to comprehensively understand not only the formation pathways of monosaccharides themselves but also those of non-target products, thereby gaining an overview of the entire reaction network.

In this study, we specifically focused on the formose reaction as a representative non-enzymatic CRN to elucidate its entire compositional landscape, including the non-target products that have received little attention. On the basis of high-resolution mass spectrometry data, we visualized the compositional distributions of target products (chemical composition $C_nH_{2n}O_n$, including branched-chain monosaccharides) and non-target products using van Krevelen (VK) diagrams and Kendrick mass defect (KMD) plots and quantitatively evaluated their evolution through numerical indicators. This approach enables a comprehensive characterization of the chemical composition of both target and non-target products without requiring the structural identification of individual compounds. The methodology was applied to reaction samples catalyzed by NaOH and $Ca(OH)_2$, and the temporal evolution of their compositional distributions was compared (Figure 1b).

Figure 2a,b show the consumption of HCHO at 80 °C when NaOH and $Ca(OH)_2$ were used as catalysts, respectively. Under $Ca(OH)_2$-catalyzed conditions, HCHO was consumed more rapidly than under NaOH catalysis. Subsequently, product analyses were conducted at four representative stages: the initial stage (Stage I, HCHO conversion: ~10%), the middle stage (Stage II, ~40%), the late stage (Stage III, ~85%), and the final stage (Stage IV, ~98%). High performance liquid chromatography (HPLC) analysis of the reaction mixtures confirmed the formation of monosaccharides at each stage and revealed that the product distributions varied depending on the catalyst used (Figure S1 and S2). The samples collected at each stage were further analyzed by the electrospray ionization in negative-ion mode–mass spectrometry (ESI(−)–MS) to evaluate the *molecular formula richness* (MFR; total number of different molecular formulas, Figures S3 and S4; Table S1),[32,33] which reflects the molecular diversity of the products. The MFR increased from 24 to 50 under NaOH catalysis and from 15 to 84 under $Ca(OH)_2$ catalysis as the reaction proceeded from Stage I to Stage IV (Figure 2c,d). At all of the stages, the MFR of non-target products (other than $C_nH_{2n}O_n$) was 4–7 times

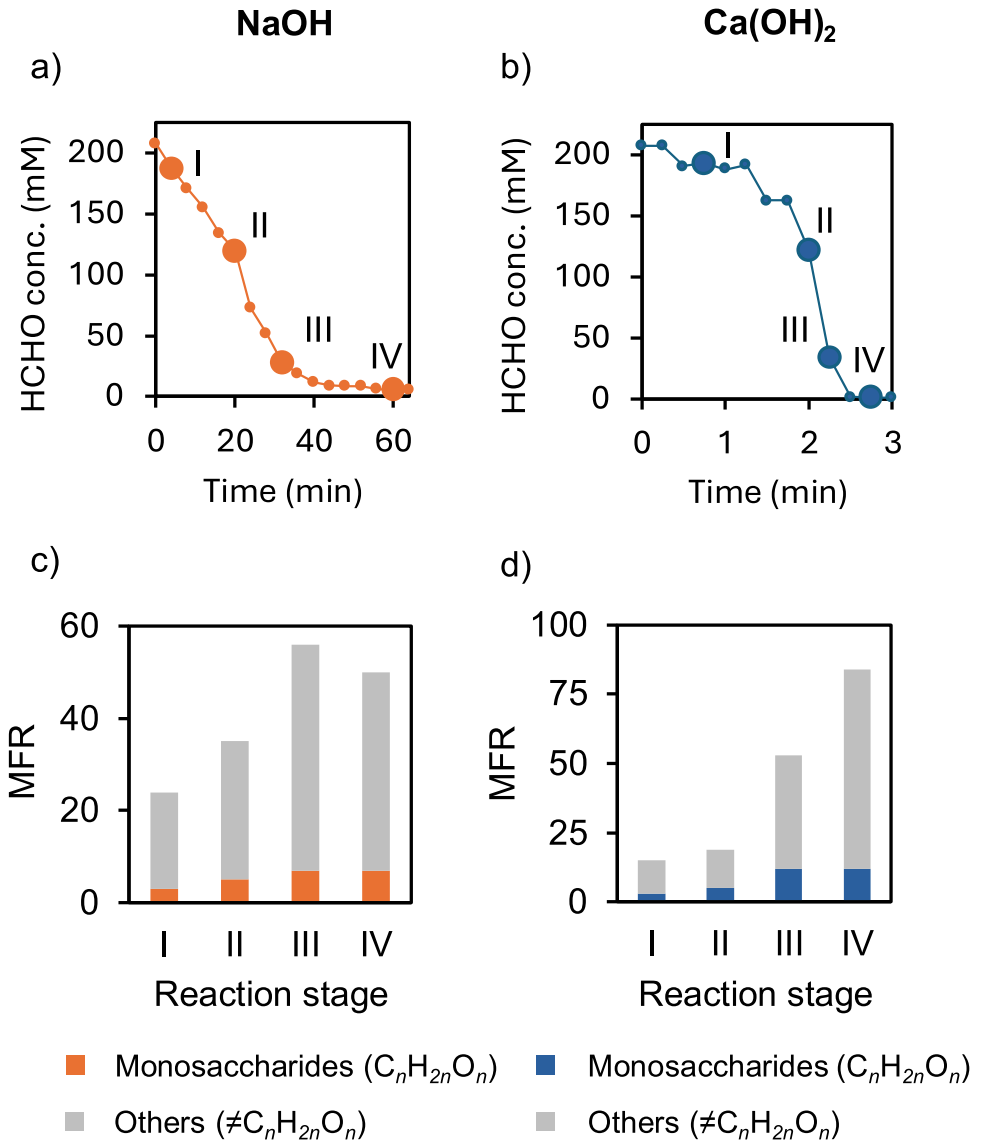

Figure 2. HCHO consumption and molecular-formula richness (MFR) at 80 °C. a), b) HCHO conversion versus time under a) NaOH and b) $Ca(OH)_2$ catalysis; large markers denote sampling points (Stages I–IV: ~10%, ~40%, ~85%, ~98%). c), d) MFR at each stage for c) NaOH and d) $Ca(OH)_2$ catalysis; orange and blue bars = monosaccharides ($C_nH_{2n}O_n$), gray = non-target species.

higher than that of monosaccharides ($C_nH_{2n}O_n$), highlighting the remarkable diversity of these non-target products. Each molecular formula corresponds to multiple isomers (both structural and stereoisomers). For instance, $C_6H_{12}O_6$ includes structural isomers such as glucose and fructose, as well as stereoisomers such as glucose and galactose. Therefore, the total number of chemical species present in the reaction mixture is expected to exceed the MFR values. Although gas chromatography–mass spectrometry (GC–MS) is generally effective for identifying compounds, its application to the formose reaction is highly challenging and labor-intensive. The analysis is confounded by an extremely large number of peaks (Figures S5 and S6), highly similar mass spectra between isomers, and the difficulty of acquiring or synthesizing standards. Consequently, rather than identifying each product individually, obtaining an overview of how the feedstock is dynamically distributed between target and non-target products provides valuable insights for understanding the formose reaction network.

In this study, we used the VK diagram and the KMD plot as methodological tools to obtain an overview of the dynamic behavior of the reaction products. In the VK diagram, compounds are mapped onto a two-dimensional plane on the basis of their elemental composition ratios (H/C and O/C), enabling the visualization of the compositional distribution of complex mixtures (Figure 3a).[34] In this plot, all monosaccharides ($C_nH_{2n}O_n$) occupy the same position at H/C = 2 and O/C = 1, hereafter referred to as the *monosaccharide coordinate*. For example, compounds formed through dehydration from monosaccharides appear toward the lower left, whereas reduced compounds are plotted upward. Thus, the VK diagram provides an intuitive visualization of the

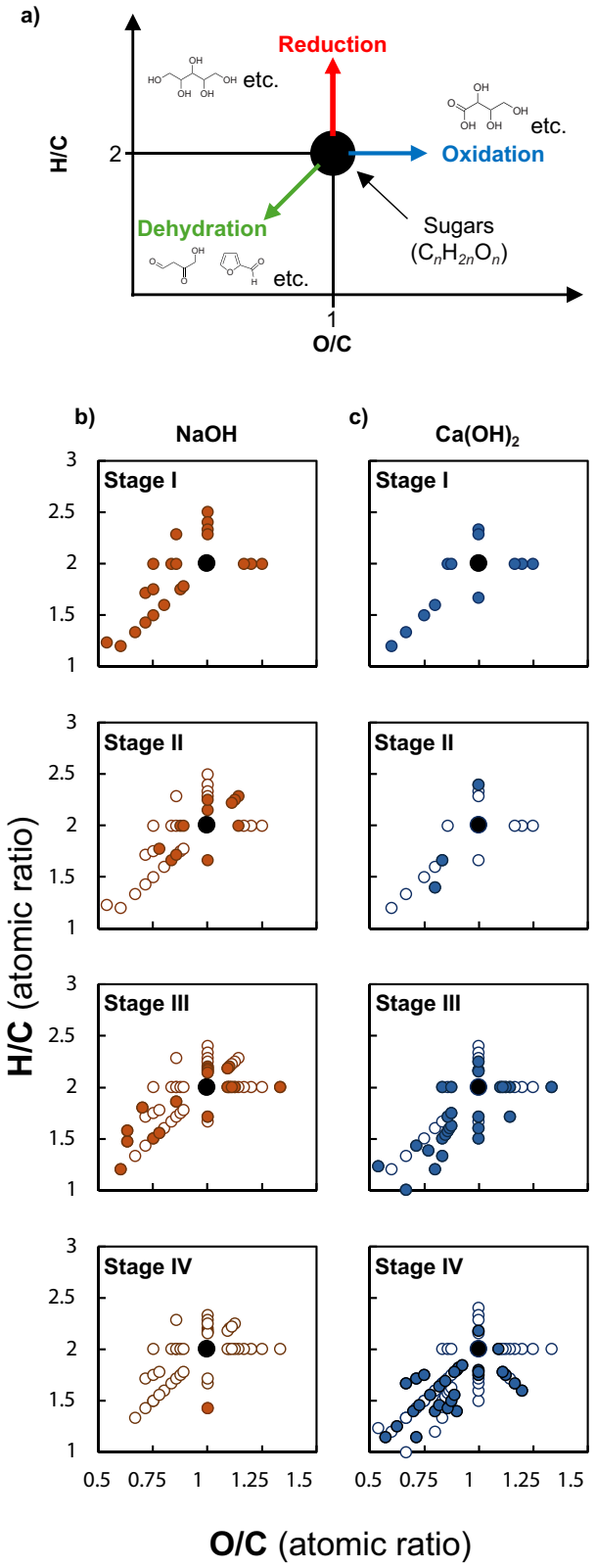

Figure 3. VK diagrams of product compositions. a) Schematic showing the monosaccharide coordinate (H/C = 2, O/C = 1) and expected shifts for reduction, oxidation, and dehydration. b), c) Stages I–IV under b) NaOH and c) $Ca(OH)_2$ catalysis; open circles = species persisting from the previous stage; filled circles = newly appearing; black circles = monosaccharides.

overall compositional trends in the formose reaction. The KMD plot visualizes structurally related compounds using the KMD and nominal Kendrick mass (NKM), calculated with a specific repeating unit (CH_2O in this study, Figure 4a).[35] In this representation, compounds that differ only in the number of CH_2O units share the same KMD value and therefore appear as horizontally aligned series (Table S2). These two analytical methods are complementary: both allow rapid and comprehensive characterization of the compositional distribution of complex mixtures on the sole basis of high-resolution mass information, without the need for separating or structurally identifying individual isomers.[36–40] While this MS-based approach offers a powerful overview of compositional diversity, it does not directly provide quantitative information, and ESI-MS is inherently susceptible to non-covalent aggregate formation. These methodological considerations are discussed in detail in the Supporting Information.

Figure 3b shows the VK diagram obtained for the reaction catalyzed by NaOH. Each point corresponds to a detected molecular formula, with newly appearing compounds (filled circles) distinguished from those that persist from the previous stage (open circles). The black point indicates the monosaccharide coordinate. In Stage I, products were observed both at the monosaccharide coordinate and other positions, visualizing the coexistence of the target product (monosaccharides) and other non-target products in this initial stage. In Stage II, the distribution expanded upward (increasing H/C ratio), rightward (increasing O/C ratio), and toward the lower left (decreasing H/C and O/C ratios) from the monosaccharide coordinate. These trends correspond to the accumulation of products formed through reduction, oxidation, and dehydration, respectively. In the late stage (Stage III), this multidirectional spread became more pronounced, clearly demonstrating the diversification of reaction products as the reaction progressed. At Stage IV, the distribution was nearly identical to that at Stage III, suggesting that the product composition was no longer substantially evolving. As shown in Figure 4b, the KMD plot exhibited a similar trend: relative to the dashed line at KMD $\approx$ 0 corresponding to monosaccharides, the plotted points expanded in both the upward and downward directions as the reaction proceeded. This expansion indicates the concurrent formation of reduced products (KMD $<$ 0) and oxidized or dehydrated products (KMD $>$ 0).

We quantitatively evaluated these qualitative trends by defining a coordinate system on the VK diagram with the monosaccharide coordinate as the origin and treating the position of each product as a position vector. Each vector was normalized, and the length of the resultant vector was calculated as the *mean resultant length* (R). The value of R ranges from 0 to 1, where smaller values indicate an isotropic distribution and larger values indicate a directional bias. For the non-target products that newly appeared between Stages I and IV under NaOH catalysis, we obtained R = 0.18, indicating a nearly isotropic distribution around the monosaccharide coordinate (Tables S3 and S4). In addition, on the basis of the KMD plot, another parameter was defined as the fraction of compounds (excluding monosaccharides,

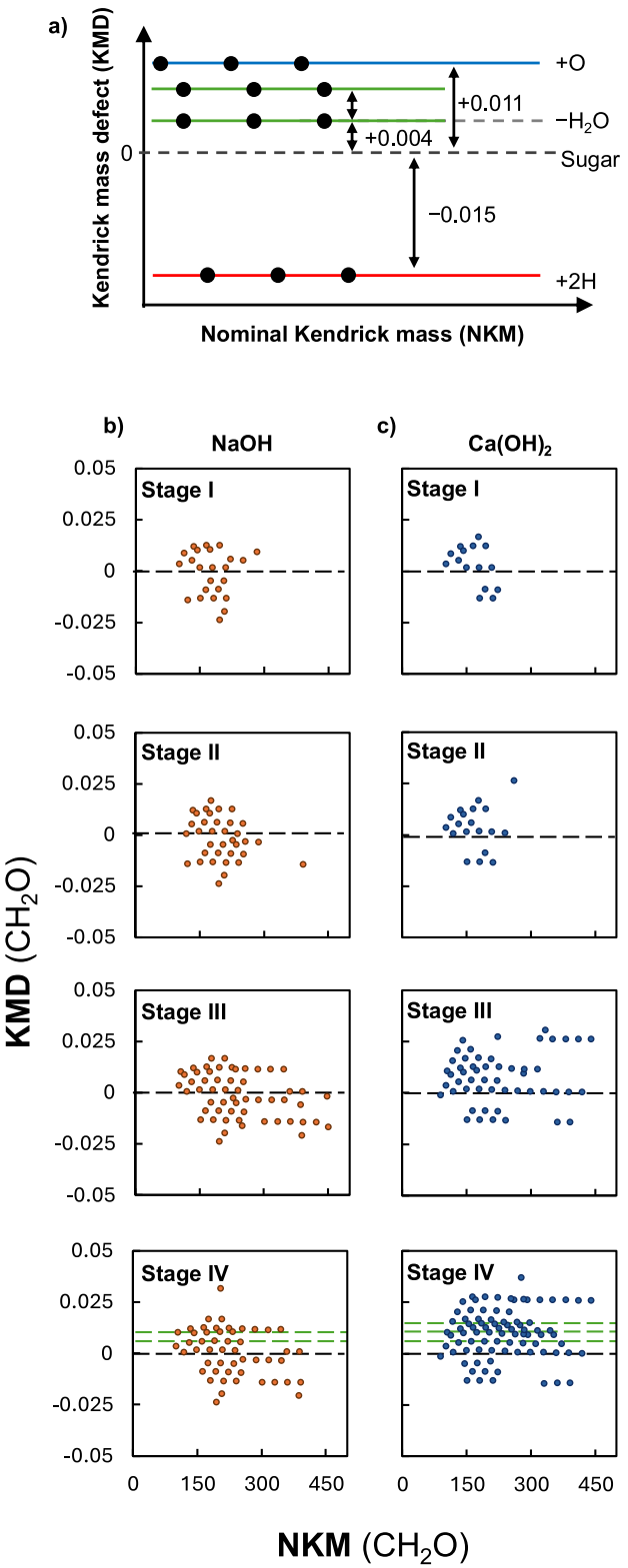

Figure 4. KMD plots (CH_2O base) of related series. a) Schematic: axes are nominal Kendrick mass (NKM) and KMD; the black dashed line (KMD ≈ 0) marks monosaccharides; lines indicate theoretical shifts for reduction, oxidation, and dehydration. b), c) Stages I–IV under b) NaOH and c) $Ca(OH)_2$ catalysis; black line = monosaccharides (KMD ≈ 0); green dashed lines highlight stepwise dehydration ($-H_2O$, $-2H_2O$, $-3H_2O$; ∼+0.004 KMD steps).

$C_nH_{2n}O_n$) with KMD > 0. This value remained constant at 40%–52%, demonstrating nearly equivalent numbers of dehydrated/oxidized and reduced compounds (Table S5).

By contrast, when $Ca(OH)_2$ was used as the catalyst, a distinctly different pattern was observed. As shown in the VK diagram (Figure 3c), the distribution in Stage I was similar to that under NaOH catalysis and the formation of monosaccharides and several non-target products was detected. In Stage II, although the number of plotted points slightly increased, the overall distribution pattern remained almost unchanged from that in Stage I, in contrast to the broad compositional expansion observed under NaOH catalysis. This lack of change in the distribution pattern indicates limited emergence of new non-target compositions during the early to middle stages. In Stage III, the distribution changed markedly, expanding anisotropically toward the lower left from the monosaccharide coordinate, indicating increased formation of dehydrated products. This trend became more pronounced in Stage IV, where dehydration-derived products were predominantly formed. Corresponding to this distinct change in the VK diagram, the KMD plot also revealed dense clustering of points in the region with KMD > 0, forming a characteristic band structure (Figure 4c). These bands were spaced at intervals of approximately 0.004 in KMD, reflecting the formation of a series of compounds with repeating CH_2O units that underwent stepwise dehydration, such as $-H_2O$, $-2H_2O$, and $-3H_2O$.

To quantitatively evaluate these observations, we calculated the same numerical indicators used for the NaOH-catalyzed system. For the set of newly appearing plots observed between Stages I and IV on the VK diagram, the mean resultant length R was 0.68, indicating a strong directional bias, in contrast to the nearly isotropic distribution observed under NaOH catalysis ($R = 0.18$) (Tables S3 and S4). The mean direction of the resultant vector was –100° (taking the positive O/C axis as 0°), in reasonable agreement with the theoretical angle for dehydration (−116.6°). In addition, the occupancy ratio of the region with KMD > 0 among the non-target products increased from 54% to 78% as the reaction progressed (Table S5). This increase contrasts with the nearly constant occupancy (∼50%) observed under NaOH catalysis. These results suggest that, under $Ca(OH)_2$ catalysis, dehydration reactions proceed predominantly from Stage III to Stage IV, leading to an increased diversity of non-target products. The distinct differences in compositional trends between the two catalytic systems are likely attributable to differences in catalytic activity, variations in pH during the reaction, and/or the contribution of monosaccharide–metal complex formation.[41–43] For example, in contrast to Na^+, which exhibits minimal specific interactions with sugars, Ca^{2+} is known to form stable complexes with monosaccharides and enediol intermediates.[44–46] Such interactions could facilitate substrate activation and thereby contribute to the preferential formation of dehydrated products under $Ca(OH)_2$ catalysis. Notably, the trends observed in both the VK diagrams and KMD plots for NaOH- and $Ca(OH)_2$-catalyzed reactions were reproduced when independently prepared samples were analyzed using different instruments (Figures S7 and S8). Furthermore, we examined additional reaction conditions under

the $Ca(OH)_2$-catalyzed system: lower temperature, reduced initiator concentration, and reduced substrate concentration. The VK diagrams revealed that certain parameters, particularly temperature, exert a pronounced influence on the product-distribution patterns (see Figures S11–S13).

Although more than half of the feedstock in the formose reaction is converted into non-target products rather than monosaccharides, these products have conventionally been collectively referred to as "tar," and their detailed characterization has rarely been attempted. At present, the individual chemical components contained in the "tar" have not yet been identified, and further investigation will be required from this perspective. However, we demonstrate for the first time that the distribution of these non-target products changes in a distinct and systematic manner depending on the catalyst species and reaction stage, as revealed by the VK diagram and KMD plot. Specifically, under NaOH catalysis, non-target products diversified isotropically on the VK diagram, whereas under $Ca(OH)_2$ catalysis, products with dehydrated compositions became predominant in the middle to late stages of the reaction. Such a comprehensive understanding of the entire reaction network enables system design that considers the formation dynamics of non-target products. For instance, because dehydration-derived non-target products markedly increase in the late stage under $Ca(OH)_2$ catalysis, halting the reaction earlier or introducing additives that suppress dehydration could reduce the carbon flux toward non-target products, thereby improving the yield of the target products. Previous studies have empirically shown that chemical intervention at intermediate reaction stages narrows the product distribution.[41]

The framework presented in this study is expected to be applicable not only to the formose reaction system but also more broadly to complex CRNs, including biological metabolic pathways. For other complex reaction networks as well, a global view of the time-evolving compositional distributions of both target and non-target products provides valuable insights into the overall behavior of the system. We anticipate that the framework developed in this study will advance future research aimed at elucidating such network-level characteristics.

Supporting Information

The authors have cited additional references within the Supporting Information.[47–49]

Acknowledgements

This work was supported by a JSPS KAKENHI Program (Grant Number 25KJ1748). Mass spectrometry measurements were performed using research equipment shared under the MEXT Project for Promoting Public Utilization of Advanced Research Infrastructure (Program for Supporting Construction of Core Facilities, Grant Number JPMXS0441200025), and the measurements were supported by Dr. Akio Hayashi.

Conflict of Interests

The authors declare no conflict of interest.

Data Availability Statement

The data that support the findings of this study are available from the corresponding author upon reasonable request.

Keywords: Carbohydrates · Chemical reaction network · Formose reaction · Mass spectrometry · Systems chemistry

[1] T. Schwander, L. Schada von Borzyskowski, S. Burgener, N. S. Cortina, T. J. Erb, *Science* **2016**, *354*, 900–904.
[2] A. Satanowski, D. G. Marchal, A. Perret, J.-L. Petit, M. Bouzon, V. Döring, I. Dubois, H. He, E. N. Smith, V. Pellouin, H. M. Petri, V. Rainaldi, M. Nattermann, S. Burgener, N. Paczia, J. Zarzycki, M. Heinemann, A. Bar-Even, T. J. Erb, *Nat. Commun.* **2025**, *16*, 3134.
[3] P. L. Türtscher, M. Reiher, *J. Chem. Inf. Model.* **2023**, *63*, 147–160.
[4] J. P. Unsleber, M. Reiher, *Annu. Rev. Phys. Chem.* **2020**, *71*, 121–142.
[5] Y. Himeoka, J. B. Kirkegaard, N. Mitarai, S. Krishna, *Sci. Rep.* **2024**, *14*, 22187.
[6] A. S. Y. Wong, W. T. S. Huck, *Beilstein J. Org. Chem.* **2017**, *13*, 1486–1497.
[7] M. G. Baltussen, T. J. de Jong, Q. Duez, W. E. Robinson, W. T. S. Huck, *Nature* **2024**, *631*, 549–555.
[8] A. Butlerow, *Justus Liebigs Annalen der Chemie* **1861**, *120*, 295–298.
[9] W. P. Huskey, I. R. Epstein, *J. Am. Chem. Soc.* **1989**, *111*, 3157–3163.
[10] A. Blokhuis, D. Lacoste, P. Nghe, *Proc. Natl. Acad. Sci. USA* **2020**, *117*, 25230–25236.
[11] W. E. Robinson, E. Daines, P. van Duppen, T. de Jong, W. T. S. Huck, *Nat. Chem.* **2022**, *14*, 623–631.
[12] R. Breslow, *Tetrahedron Lett.* **1959**, *1*, 22–26.
[13] A. Hashidzume, *BBA Advances* **2025**, *7*, 100141.
[14] A. Ricardo, F. Frye, M. A. Carrigan, J. D. Tipton, D. H. Powell, S. A. Benner, *J. Org. Chem.* **2006**, *71*, 9503–9505.
[15] A. N. Simonov, O. P. Pestunova, L. G. Matvienko, V. N. Parmon, *Kinet. Catal.* **2007**, *48*, 245–254.
[16] A. K. Eckhardt, M. M. Linden, R. C. Wende, B. Bernhardt, P. R. Schreiner, *Nat. Chem.* **2018**, *10*, 1141–1147.
[17] Q. P. Tran, R. Yi, A. C. Fahrenbach, *Chem. Sci.* **2023**, *14*, 9589–9599.
[18] S. Lamour, S. Pallmann, M. Haas, O. Trapp, *Life* **2019**, *9*, 52.
[19] H.-J. Kim, A. Ricardo, H. I. Illangkoon, M. J. Kim, M. A. Carrigan, F. Frye, S. A. Benner, *J. Am. Chem. Soc.* **2011**, *133*, 9457–9468.
[20] P. van Duppen, E. Daines, W. E. Robinson, W. T. S. Huck, *J. Am. Chem. Soc.* **2023**, *145*, 7559–7568.
[21] T. J. de Jong, A. D. Demertzi, W. E. Robinson, W. T. S. Huck, *Angew. Chem. Int. Ed.* **2025**, *64*, e202504659.
[22] N. E. Soland, I. Roh, W.-S. Huynh, P. Yang, *ACS Sustainable Chem. Eng.* **2023**, *11*, 12478–12483.
[23] N. Soland, J. Luo, A. L. Maulana, J. Feijoo, H.-J. Jo, A. M. Oddo, Y. Shan, T. Wang, G. Lee, J. Choi, W.-S. Huynh, M. F. Guzman, L. Jayasinghe, C. Zhu, Y. Yang, P. Yang, *Proc. Natl. Acad. Sci. USA* **2025**, *122*, e2514826122.

[24] J. Deng, T. Pan, Q. Xu, M.-Y. Chen, Y. Zhang, Q.-X. Guo, Y. Fu, *Sci. Rep.* **2013**, *3*, 1244.
[25] S. Cestellos-Blanco, S. Louisia, M. B. Ross, Y. Li, N. E. Soland, T. C. Detomasi, J. N. Cestellos Spradlin, D. K. Nomura, P. Yang, *Joule* **2022**, *6*, 2304–2323.
[26] H. Tabata, G. Chikatani, H. Nishijima, T. Harada, R. Miyake, S. Kato, K. Igarashi, Y. Mukouyama, S. Shirai, M. Waki, Y. Hase, S. Nakanishi, *Chem. Sci.* **2023**, *14*, 13475–13484.
[27] A. Omran, C. Menor-Salvan, G. Springsteen, M. Pasek, *Life* **2020**, *10*, 125.
[28] H. G. Hansma, *Orig. Life Evol. Biosph.* **2014**, *44*, 307–311.
[29] K. Paschek, K. Kohler, B. K. D. Pearce, K. Lange, T. K. Henning, O. Trapp, R. E. Pudritz, D. A. Semenov, *Life* **2022**, *12*.
[30] A. A. Pogodaev, T. T. Lap, W. T. S. Huck, *ChemSystemsChem* **2021**, *3*, e2000033.
[31] W. Zhang, Y. Wang, K. R. Rout, T. Margossian, D. Chen, *Ind. Eng. Chem. Res.* **2024**, *63*, 9419–9424.
[32] A. Mentges, C. Feenders, M. Seibt, B. Blasius, T. Dittmar, *Front. Mar. Sci.* **2017**, *4*, 194.
[33] Y. Cui, S. Wen, J. C. Stegen, A. Hu, J. Wang, *Water Res.* **2024**, *250*, 121054.
[34] V. Krevelen, *Fuel* **1950**, *29*, 269–284.
[35] E. Kendrick, *Anal. Chem.* **1963**, *35*, 2146–2154.
[36] W. Kew, I. Goodall, D. Clarke, D. Uhrín, *J. Am. Soc. Mass Spectrom.* **2017**, *28*, 200–213.
[37] S. Merel, *Chemosphere* **2023**, *313*, 137443.
[38] S. Wang, Y. Wang, Z. Shi, K. Sun, Y. Wen, L. Niedzwiecki, R. Pan, Y. Xu, I. N. Zaini, K. Jagodzińska, C. Aragon-Briceno, C. Tang, T. Onsree, N. Tippayawong, H. Pawlak-Kruczek, P. G. Jönsson, W. Yang, J. Jiang, S. Kawi, C.-H. Wang, *Commun. Chem.* **2023**, *6*, 273.
[39] J. R. Laszakovits, A. A. MacKay, *J. Am. Soc. Mass Spectrom.* **2022**, *33*, 198–202.
[40] L. Blanc, G. B. Ferraro, M. Tuck, B. Prideaux, V. Dartois, R. K. Jain, N. Desbenoit, *Anal. Chem.* **2021**, *93*, 16314–16319.
[41] Y. Shigemasa, M. Kawahara, C. Sakazawa, R. Nakashima, T. Matsuura, *J. Catal.* **1980**, *62*, 107–116.
[42] Y. Shigemasa, T. Taji, E. Waki, R. Nakashima, *Bull. Chem. Soc. Jpn.* **1981**, *54*, 1403–1409.
[43] A. Venturini, J. González, *ChemPlusChem* **2024**, *89*, e202300388.
[44] A. H. Weiss, T. John, *J. Catal.* **1974**, *32*, 216–229.
[45] K. Fujino, J.-i. Kobayashi, I. Higuchi, *NIPPON KAGAKU KAISHI* **1972**, *1972*, 2287–2292.
[46] A. Pallagi, É. G. Bajnóczi, S. E. Canton, T. Bolin, G. Peintler, B. Kutus, Z. Kele, I. Pálinkó, P. Sipos, *Environ. Sci. Technol.* **2014**, *48*, 6604–6611.
[47] T. Zweckmair, S. Böhmdorfer, A. Bogolitsyna, T. Rosenau, A. Potthast, S. Novalin, *J. Chromatogr. Sci.* **2014**, *52*, 169–175.
[48] S. M. Sutton, S. Pulletikurti, H. Lin, R. Krishnamurthy, C. L. Liotta, *Chem* **2025**, *11*, 102553.
[49] M. Q. Edwards, D. T. Holden, R. G. Cooks, *Chem. Sci.* **2025**, *16*, 7057–7065.

Manuscript received: November 15, 2025
Revised manuscript received: December 08, 2025
Manuscript accepted: December 19, 2025
Version of record online: ■■, ■■